JOURNAL OF SYNCHROTRON RADIATION

ISSN 1600-5775

A miniature closed-circle flow cell for high photon flux X-ray scattering experiments

Ch. J. Sahle,[a]* C. Henriquet,[a] M. A. Schroer,[b,c] I. Juurinen,[d] J. Niskanen[d] and M. Krisch[a]

[a]ESRF – The European Synchrotron, CS 40220, 38043 Grenoble Cedex 9, France, [b]Deutsches Elektronen-Synchrotron DESY, Notkestrasse 85, 22607 Hamburg, Germany, [c]The Hamburg Centre for Ultrafast Imaging (CUI), Luruper Chaussee 149, 22761 Hamburg, Germany, and [d]Department of Physics, University of Helsinki, Helsinki, Finland. *Correspondence e-mail: christoph.sahle@esrf.fr

Received 15 June 2015
Accepted 1 September 2015

Edited by S. M. Heald, Argonne National Laboratory, USA

Keywords: inelastic X-ray scattering; sample environments; radiation damage; liquids.

A closed-circle miniature flow cell for high X-ray photon flux experiments on radiation-sensitive liquid samples is presented. The compact cell is made from highly inert material and the flow is induced by a rotating magnetic stir bar, which acts as a centrifugal pump inside the cell. The cell is ideal for radiation-sensitive yet precious or hazardous liquid samples, such as concentrated acids or bases. As a demonstration of the cell's capabilities, X-ray Raman scattering spectroscopy data on the oxygen *K*-edge of liquid water under ambient conditions are presented.

1. Introduction

X-ray scattering experiments are indispensable for both fundamental research and the applied sciences (Als-Nielsen & McMorrow, 2011; Willmott, 2011). Modern X-ray sources, such as third-generation synchrotron radiation facilities, nowadays enable experiments even with extremely low scattering cross sections.

One rapidly evolving scattering technique with such a small cross section is X-ray Raman scattering (XRS) spectroscopy, which is often also called non-resonant inelastic X-ray scattering of core electrons, where the intensity of scattered hard X-rays is recorded as a function of their energy loss and momentum transfer (Schülke, 2007). A striking advantage of hard X-ray techniques compared with soft X-ray methods is their capability to probe samples under well defined and tunable thermodynamic conditions (p, T) where the sample can be guaranteed to be in thermodynamic equilibrium. The XRS method allows also for probing of dipole-forbidden transitions by tuning the parameters of the scattering experiment. For example, XRS experiments on liquid samples have been performed utilizing these advantages (Pylkkänen *et al.*, 2010, 2011; Sahle *et al.*, 2013; Juurinen *et al.*, 2013, 2014). However, the enormous doses of energetic radiation necessary for these experiments often compromises the integrity of many samples (Mao *et al.*, 2006). In macromolecular crystallography, samples are cooled to cryogenic temperatures to lessen the damaging effects of hard X-rays (Ravelli & Garman, 2006). For liquid samples, cooling, of course, is not an option and radiation damage in radiation-sensitive fluids is often circumvented by producing a liquid flow through the X-ray beam such that the sample molecules only shortly interact with the X-ray beam. If samples are available in large quantities, it is most convenient to use large volumes of sample and either circulate the sample or flush them throughout the

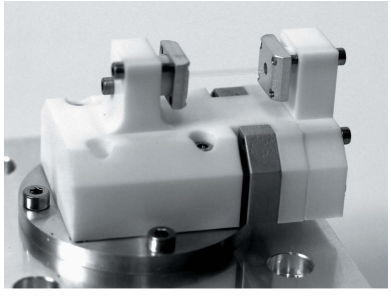

experiment, *e.g.* using a peristaltic pump setup (Pylkkänen *et al.*, 2010, 2011; Juurinen *et al.*, 2013, 2014) or liquid jet (Chapman *et al.*, 2011). However, sometimes samples are not available in large quantities (*e.g.* precious samples or samples which are difficult to synthesize in larger quantities) or large quantities of sample are not advisable, *e.g.* samples that pose a safety hazard (such as strong acids or bases). In these cases, flow systems that use large sample volumes are not desirable.

Here we present a new small-scale closed-circle liquid flow cell for experiments that necessitate high photon flux densities, such as XRS experiments. The design of the cell is simple and compact and allows for a large range of scattering angles. Different cell body and capillary materials enable a wide variety of liquids including strong acids and bases. The functionality of the cell is based on a small magnetic stir bar, which is driven by a rotating permanent magnet outside the cell. This stir bar acts as a miniature centrifugal pump. For demonstration purposes, we will show XRS spectra of the oxygen *K*-edge of liquid water under ambient conditions.

2. Experimental

Fig. 1(*a*) shows a drawing (cut through the vertical plane) of the technical design of the cell. A close-up photograph of the cell is shown in Fig. 1(*b*) and a photograph of the cell mounted on the goniometer of ID20 at the ESRF is provided in Fig. 1(*c*). The propulsion of the sample liquid is achieved by a miniature built-in pump comprised of a small conventional magnetic stir fish (Conrad *et al.*, 2009) [green piece in the Fig. 1(*a*)] commonly found in chemistry laboratories to agitate liquids. The stir fish is rotated by a magnet placed on the outside of the sample cell, which is driven by an electric DC motor. The rotating magnetic stir bar acts as the impeller of a centrifugal pump. The liquid sample is fed to the center of rotation of the stir fish and the fluid exits the pump tangentially. The canals have a diameter of 2 mm. The X-ray interaction region is designed to be a capillary of 2 mm outer diameter placed in the horizontal plane. This allows us to freely choose the scattering angles in the vertical direction and the length of the capillary gives enough freedom of choice of scattering angle in the horizontal scattering plane since the X-ray polarization of the incident beam prohibits scattering angles close to $2\theta = 90^\circ$ in the horizontal plane. Depending on the speed of rotation of the permanent magnet, liquid flows of up to 200 ml min^{-1} can be achieved. The total sample volume of the cell as shown in Fig. 1 is 7 ml.

For all pumping speeds and samples tested, the liquids flowed through the system in a stable and bubble-free manner. Depending on the purpose of the experiment and the samples used, different cell body and capillary materials are possible. For the capillary, Kapton or quartz glass are convenient; for the cell body, PTFE, aluminium or stainless steel are suitable materials. We can imagine that an alternative design (*e.g.* without a capillary) would allow even for pressures of a few atmospheres, *e.g.* by using a hydrostatic pump as in Krywka *et al.* (2008) to create high-pressure conditions. For demonstration purposes, we used the cell to measure non-resonant inelastic X-ray scattering spectra of water in the vicinity of the oxygen *K*-edge. XRS is a photon-hungry technique where electronic excitations are probed by inelastic scattering of high-energy photons. The measured quantity is the double differential scattering cross section (DDSCS),

$$\frac{\mathrm{d}^2\sigma}{\mathrm{d}\Omega\,\mathrm{d}\omega} = \left(\frac{\mathrm{d}\sigma}{\mathrm{d}\Omega}\right)_{\mathrm{Th}} \frac{\omega_2}{\omega_1}\,\langle S(\mathbf{q},\omega,\mathbf{R})\rangle_{\mathrm{NpT}}, \qquad (1)$$

where $(\mathrm{d}\sigma/\mathrm{d}\Omega)_{\mathrm{Th}}$ is Thomson's scattering cross section that describes the coupling of the photons (ω_1 is the photon energy of the incoming, ω_2 that of the scattered photon) to the scattering electron system, and $S(\mathbf{q},\omega,\mathbf{R})$ is the so-called dynamic structure factor, which depends on the system's instantaneous configuration $\mathbf{R}$ and which holds all information about the sample accessible with XRS. $\langle\ldots\rangle_{\mathrm{NpT}}$ denotes the thermodynamic NpT-ensemble average. The dynamic structure factor is given by

$$S(\mathbf{q},\omega,\mathbf{R}) = \sum_{\mathrm{f}} \left|\langle \mathrm{f},\mathbf{R}|\exp(i\mathbf{q}\cdot\mathbf{r})|\mathrm{i},\mathbf{R}\rangle\right|^2 \delta(E_{\mathrm{i}} - E_{\mathrm{f}} + \hbar\omega). \qquad (2)$$

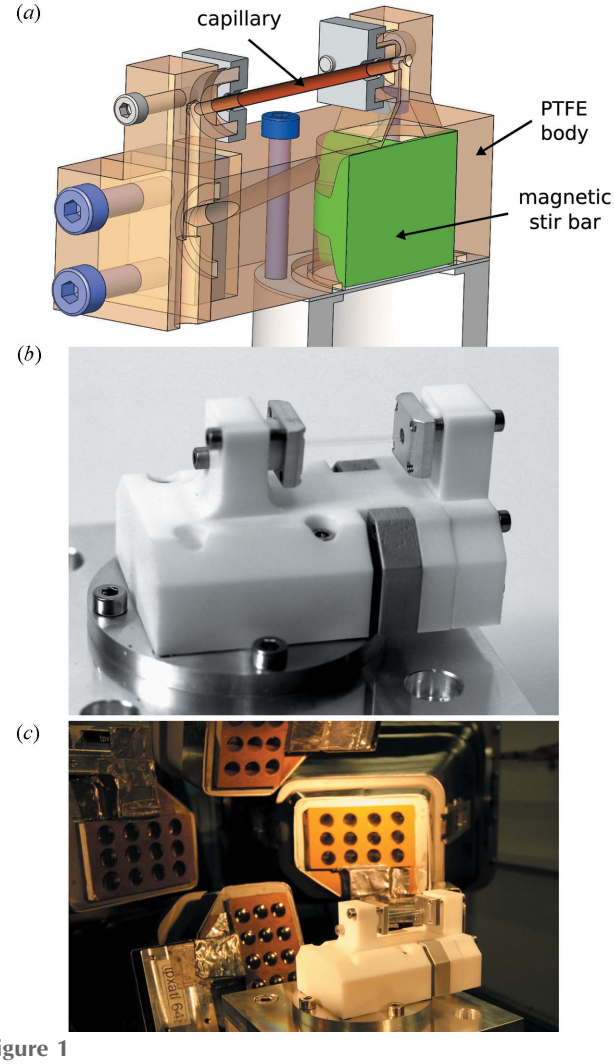

Figure 1
(*a*) Schematic drawing of the flow cell design. The magnetic stir bar is shown in green. (*b*) Photographic close-up view of the sample cell. (*c*) The flow cell mounted on the sample goniometer at ID20 of the ESRF.

Here, $|f\rangle$ and $|i\rangle$ are the final and initial state of the system, $\mathbf{q}$ is the momentum transferred to the scattering system. E_i and E_f are the energies of the initial and final state and $\hbar\omega = E_i - E_f$ is the energy transferred to the system, *i.e.* the delta function in (2) ensures energy conservation. Since there is no translational or rotational symmetry in most liquids, $\mathbf{q}$ in $S(\mathbf{q}, \omega, \mathbf{R})$ reduces to $q = |\mathbf{q}|$. With this technique, usually absorption edges of low-Z elements, such as the oxygen, carbon and nitrogen K-edges, are probed. The advantage of XRS is that the transition energies probed do not depend on the incident energy (only the energy loss has to be of the order of such absorption edges) so that hard X-rays can be used to probe these edges. This allows one to study liquid samples under ambient or even high pressure and temperature conditions (Sahle *et al.*, 2013).

Owing to the momentum transfer dependence of XRS, one can probe final states of different symmetries, *i.e.* one is not limited to dipolar transitions. The information gained for low momentum transfers is analogous (Mizuno & Ohmura, 1967) to the X-ray absorption near-edge structure (XANES), and even the extended X-ray absorption fine structure (EXAFS) is accessible (Huotari *et al.*, 2012). At higher momentum transfer values the measured cross section (2) is sensitive to dipole forbidden transitions. Studies of the high-order multiplet features in the 3*d* transition metals, rare earths and actinides are examples of how to exploit this fact (Gordon *et al.*, 2008; Caciuffo *et al.*, 2010; Sen Gupta *et al.*, 2011; Huotari *et al.*, 2015). Information from different excitation channels provides access to the entire unoccupied density of states (Soininen *et al.*, 2005; Inkinen *et al.*, 2014).

The spectra shown in this contribution were measured at the inelastic X-ray scattering beamline ID20 of the European Synchrotron Radiation Facility (ESRF), Grenoble, France. This beamline has four consecutive undulators producing a pink beam. The incoming X-ray radiation was monochromated in two stages. First, a high-heat-load Si(111) monochromator reduces the bandwidth of the incoming X-rays to some 1.4 eV. Secondly, we used a Si(311) channel-cut monochromator to further reduce the bandwidth to 0.3 eV. Using a mirror system in Kirkpatrick–Baez geometry, the incident beam was focused to a spot size of 20 µm (V) × 10 µm (H) at the position of the sample leading to a photon flux density of 10^9 photons s^{-1} mm^{-2}. The sample cell was placed on a 500 mm-radius Rowland circle and the inelastically scattered photons were analyzed using 36 spherically bent Si(110) crystals in forward-scattering geometry (see Fig. 1*c*). We used the Si(660) reflection at 9.7 keV, and the energy- and momentum-resolved photons were detected using three photon-counting Maxipix Timepix detectors. The overall energy resolution (FWHM of the quasielastic line of the sample) was 0.65 eV. The X-ray exposure time per energy loss point was 5 s and the overall counting time (including times for motor movements) was 12 min per spectrum. During motor movements and detector readout the incident beam was blocked by a fast attenuator.

Fig. 2 shows images of a detector region (*ca.* 40 × 20 pixels), onto which scattering of the liquid water sample from a single analyzer crystal is focused, at different times during an inelastic X-ray scattering measurement. The highlighted (yellow and red) region on each image depicts a real-space image of the X-ray beam as it impinges through the liquid water sample (Huotari *et al.*, 2011; Sahle *et al.*, 2015). The images in the left-hand column of the figure were taken during an energy scan without flow and we could observe a gas bubble forming due to radiation damage (marked with an arrow) after approximately 150 s of exposure to the X-rays. When engaging a flow (right column), we could not observe any bubble formation throughout the duration of the experiment. This demonstration underlines the importance of a flow when measuring liquid samples and also demonstrates the usefulness of area detectors to monitor the sample's integrity during XRS experiments.

To obtain an XRS spectrum, the incident photon energy is scanned at fixed analyzer energy to create an energy-loss spectrum (so-called inverse geometry). Images such as those shown in Fig. 2 are recorded for each energy-loss point desired and pixels from within the foci of each analyzer crystal are

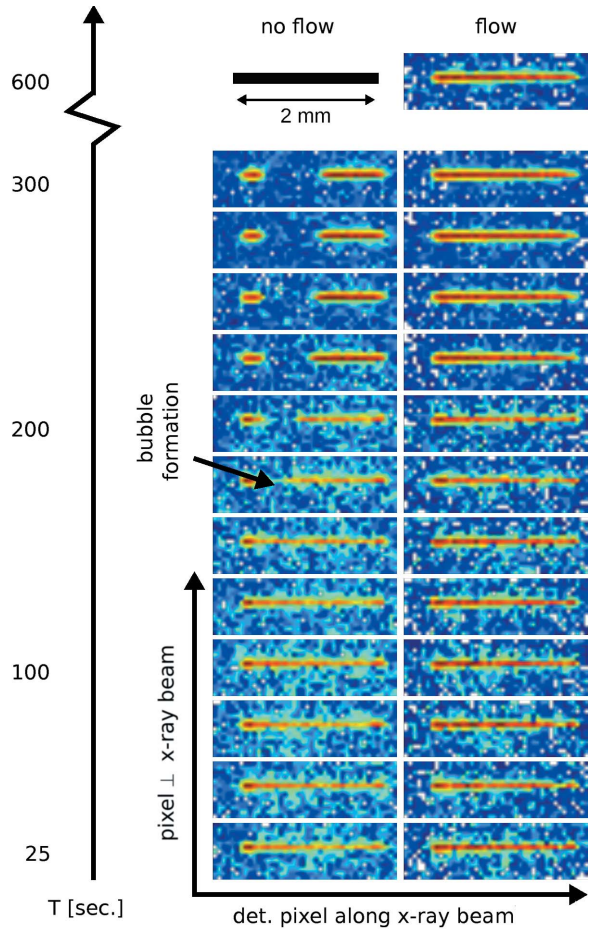

Figure 2
Collection of a zoomed-in region of detector images collected during an energy scan using the flow cell without flow (left column) and with flow (right column). Without flow, one can clearly observe a bubble forming after *ca.* 150 s of exposure to X-rays (black arrow). Each image depicts a real-space image of the X-ray beam as it impinges through the liquid water sample in the direction perpendicular to the water flow through a quartz glass capillary, the diameter of which is 2 mm.

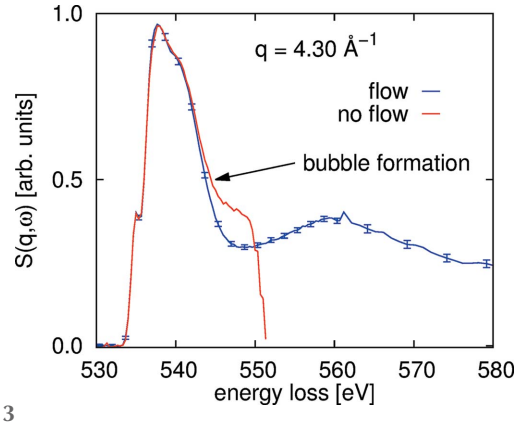

Figure 3
Oxygen *K*-edge spectrum of water at room temperature as measured from the new miniature flow cell setup without flow (red line) and with flow (blue line). The shown spectra are averages over signals from 48 analyzer crystals from a single energy scan. The collection time of the scan was 12 min. The average momentum transfer was q = 4.3 Å^{-1}. See text for details.

summed up. The XRS spectra resulting from summation of regions of interest such as shown in Fig. 2 for 36 analyzer crystals in the forward-scattering geometry (low momentum transfer) are shown in Fig. 3. The scattering angles of these 36 analyzer crystals varied between 40° and 60° resulting in an average momentum transfer of 4.3 ± 0.1 Å^{-1}. For the near-edge measurement, we covered an energy range of 40 eV over which we took 120 points and accumulated scattering intensities for 5 s per point for the samples. Bubble formation (evident from the images in Fig. 2) leads to a complete loss of intensity around 550 eV when measuring the steady sample (red line in Fig. 3). The spectrum of the sample flowing through the cell at *ca.* 50 ml min^{-1}, on the other hand, is well in agreement with *K*-edge spectra of liquid water from the literature (Wernet *et al.*, 2004; Pylkkänen *et al.*, 2011; Sahle *et al.*, 2013).

3. Conclusions and outlook

To summarize, we have presented a small, cheap and compact flow cell to allow photon-intense X-ray scattering experiments on delicate or precious and/or hazardous liquid samples. The entire solid angle of detection of the 72-analyzer-crystal spectrometer of ID20 is accessible with this cell design. For demonstration purposes we collected XRS data from liquid water under ambient conditions. The simple design of this cell makes it readily adaptable for various high photon flux experiments even under more demanding settings such as non-ambient temperatures and pressures.

Acknowledgements

We thank the European Synchrotron Radiation Facility for providing synchrotron radiation and the technical and scientific staff of ESRF beamline ID20 for support and valuable discussions. MAS thanks the excellence cluster 'The Hamburg Centre for Ultrafast Imaging – Structure, Dynamics and Control of Matter at the Atomic Scale' of the DFG. We acknowledge A. Al-Zein and M. Moretti-Sala for advice and support during the experiment and T. Pylkkänen, C. Sternemann and S. Huotari for discussions.

References

Als-Nielsen, J. & McMorrow, D. (2011). *Elements of Modern X-ray Physics*. New York: John Wiley and Sons.
Caciuffo, R., van der Laan, G., Simonelli, L., Vitova, T., Mazzoli, C., Denecke, M. A. & Lander, G. H. (2010). *Phys. Rev. B*, **81**, 195104.
Chapman, H. N. P. *et al.* (2011). *Nature (London)*, **470**, 73–77.
Conrad, H., Lehmkühler, F., Sternemann, C., Feroughi, O., Simonelli, L., Huotari, S. & Tolan, M. (2009). *Rev. Sci. Instrum.* **80**, 026103.
Gordon, R. A., Seidler, G. T., Fister, T. T., Haverkort, M. W., Sawatzky, G. A., Tanaka, A. & Sham, T. K. (2008). *Europhys. Lett.* **81**, 26004.
Huotari, S., Pylkkänen, T., Soininen, J. A., Kas, J. J., Hämäläinen, K. & Monaco, G. (2012). *J. Synchrotron Rad.* **19**, 106–113.
Huotari, S., Pylkkänen, T., Verbeni, R., Monaco, G. & Hämäläinen, K. (2011). *Nat. Mater.* **10**, 489–493.
Huotari, S., Suljoti, E., Sahle, Ch. J., Rädel, S., Monaco, G. & de Groot, F. M. F. (2015). *New J. Phys.* **17**, 043041.
Inkinen, J., Niskanen, J., Sakko, A., Ruotsalainen, K. O., Pylkkänen, T., Galambosi, S., Hakala, M., Monaco, G., Hämäläinen, K. & Huotari, S. (2014). *J. Phys. Chem. A*, **118**, 3288–3294.
Juurinen, I., Pylkkänen, T., Ruotsalainen, K. O., Sahle, Ch. J., Monaco, G., Hämäläinen, K., Huotari, S. & Hakala, M. (2013). *J. Phys. Chem. B*, **117**, 16506–16511.
Juurinen, I., Pylkkänen, T., Sahle, Ch. J., Simonelli, L., Hämäläinen, K., Huotari, S. & Hakala, M. O. (2014). *J. Phys. Chem. B*, **118**, 5518.
Krywka, C., Sternemann, C., Paulus, M., Tolan, M., Royer, C. & Winter, R. (2008). *ChemPhysChem*, **9**, 2809–2815.
Mao, W. L., Mao, H., Meng, Y., Eng, P. J., Hu, M. Y., Chow, P., Cai, Y. Q., Shu, J. & Hemley, R. J. (2006). *Science*, **314**, 636–638.
Mizuno, Y. & Ohmura, Y. (1967). *J. Phys. Soc. Jpn*, **22**, 445–449.
Pylkkänen, T., Lehtola, J., Hakala, M., Sakko, A., Monaco, G., Huotari, S. & Hämäläinen, K. (2010). *J. Phys. Chem. B*, **114**, 13076–13083.
Pylkkänen, T., Sakko, A., Hakala, M., Hämäläinen, K., Monaco, G. & Huotari, S. (2011). *J. Phys. Chem. B*, **115**, 14544–14550.
Ravelli, R. B. G. & Garman, E. F. (2006). *Curr. Opin. Struct. Biol.* **16**, 624–629.
Sahle, Ch. J., Mirone, A., Niskanen, J., Inkinen, J., Krisch, M. & Huotari, S. (2015). *J. Synchrotron Rad.* **22**, 400–409.
Sahle, Ch. J., Sternemann, Ch., Schmidt, S., Lehtola, S., Jahn, L., Simonelli, S., Huotari, S., Hakala, M., Pylkkänen, T., Nyrow, A., Mende, K., Tolan, M., Hämäläinen, K. & Wilke, M. (2013). *Proc. Natl Acad. Sci.* **110**, 6301–6306.
Schülke, W. (2007). *Electron Dynamics by Inelastic X-ray Scattering*. Oxford University Press.
Sen Gupta, S., Bradley, J. A., Haverkort, M. W., Seidler, G. T., Tanaka, A. & Sawatzky, G. A. (2011). *Phys. Rev. B*, **84**, 075134.
Soininen, J. A., Ankudinov, A. L. & Rehr, J. J. (2005). *Phys. Rev. B*, **72**, 045136.
Wernet, Ph., Nordlund, D., Bergmann, U., Cavalleri, M., Odelius, M., Ogasawara, H., Näslund, L. A., Hirsch, T. K., Ojamäe, L., Glatzel, P., Pettersson, L. G. & Nilsson, A. (2004). *Science*, **304**, 995–999.
Willmott, P. (2011). *An Introduction to Synchrotron Radiation: Techniques and Applications*. New York: John Wiley and Sons.